Effect of Substrate on the Pre-Steady-State Kinetics of the Na^+/Glucose Cotransporter

Dominique G. Gagnon, Carole Frindel, and Jean-Yves Lapointe
Groupe d'étude des protéines membranaires, Université de Montréal, Montreal, Quebec, Canada

ABSTRACT When measuring Na^+/glucose cotransporter (SGLT1) activity in *Xenopus* oocytes with the two-electrode voltage-clamp technique, pre-steady-state currents dissipate completely in the presence of saturating α-methyl-glucose (αMG, a nonhydrolyzable glucose analog) concentrations. In sharp contrast, two SGLT1 mutants (C255A and C511A) that lack a recently identified disulfide bridge express the pre-steady-state currents in the presence of αMG. The dose-dependent effects of αMG on pre-steady-state currents were studied for wild-type (wt) SGLT1 and for the two mutants. Increases in αMG concentration reduced the total transferred charge (partially for the mutants, totally for wt SGLT1), shifted the transferred charge versus membrane potential (Q-V) curve toward positive potentials, and significantly modified the time constants of the pre-steady-state currents. A five-state kinetic model is proposed to quantitatively explain the effect of αMG on pre-steady-state currents. This analysis reveals that the reorientation of free transporter is the slowest step for wt SGLT1 either in the presence or in the absence of αMG. In contrast, the conformational change of the fully loaded mutant transporters constitutes their rate-limiting step in the presence of substrate and explains the persistence of pre-steady-state currents in this situation.

INTRODUCTION

The Na^+/glucose cotransporter SGLT1 is a member of the SLC5 family and has been the archetype of this class of Na^+-coupled substrate transporters. Soon after its cloning (1), expression in *Xenopus* oocytes enabled the measurement of pre-steady-state currents, i.e., transient currents observed in the absence of substrate, which were suggestive of gating currents observed in voltage-dependent channels. As these currents were Na^+ dependent and were absent in the presence of the specific inhibitor phlorizin (Pz) or in the presence of glucose, they were considered to represent charge displacements occurring during the voltage-dependent reorientation of the Na^+-binding site and upon Na^+ binding (2).

Pre-steady-state currents have been extremely useful for devising a credible transport mechanism, with quantitative estimation of the rate constants linking the different conformational states. The original model (2) proposed in 1992 has been challenged both theoretically and experimentally ((3–8); for review see Wright and Turk (9)), and new steps have been proposed. Recently Loo et al., using fluorescently labeled mutants (10), have reported extremely slow conformational changes (time constants on the order of 100 ms) which have yet to be quantitatively explained by any proposed kinetic model. In particular, this observation is incompatible with a rate-limiting step of 50 s^{-1}, which was proposed for the translocation of the fully loaded transporter in the human isoform of SGLT1 (hSGLT1) (2,11).

One characteristic observed for nearly all cotransporters studied (Na^+/glucose cotransporters SGLT1 and SGLT2, Na^+/myo-inositol cotransporters SMIT1 and SMIT2, Na^+/monocarboxylate cotransporter SMCT1, Na^+/Pi cotransporter NaPiII, Na^+/I^- symporter NIS, gamma-aminobutyric acid transporters GAT1 and GAT3, H^+/hexose cotransporter STP1, and Cl^--dependant K^+/amino acids transporter KAAT1) is that addition of a saturating concentration of substrate leads to the total inhibition of pre-steady-state currents (11–25). Surprisingly, with the exception of GAT1, no quantitative explanation has been proposed to explain this phenomenon.

Recently, we identified a disulfide bridge between C255 and C511 in hSGLT1 (26). An interesting feature of mutants C255A and C511A, which we have not previously published, is that they express pre-steady-state currents in the presence of a saturating αMG concentration, in contrast to what is observed with wild-type (wt) SGLT1. This phenomenon has prompted us to examine the dose-dependent effects of αMG on the pre-steady-state currents for the two mutants as well as for wt SGLT1 and to propose a quantitative explanation using a kinetic model displaying different rate-limiting steps for the wt SGLT1 and the mutant cotransporters.

MATERIALS AND METHODS

Oocyte preparation and injection

Oocytes were surgically removed from *Xenopus laevis* frogs, dissected, and defolliculated as described previously (27). One day after defolliculation, oocytes were injected with 46 nl of water containing mRNA (0.1 μg/μl and 0.25 μg/μl for wt SGLT1 and mutants, respectively) to obtain maximal protein expression. Oocytes were maintained in Barth's solution (in mM: 90 NaCl, 3 KCl, 0.82 $MgSO_4$, 0.41 $CaCl_2$, 0.33 $Ca(NO_3)_2$, 5 Hepes, pH 7.6) supplemented with 5% horse serum, 2.5 mM Na^+ pyruvate, 100 units/ml

Submitted June 26, 2006, and accepted for publication October 5, 2006.

Address reprint requests to J.-Y. Lapointe, Groupe d'étude des protéines membranaires (GÉPROM), Université de Montréal, C.P. 6128, succ. Centre-ville, Montréal, Québec H3C 3J7, Canada. Tel.: 514-343-7046; Fax: 514-343-7146; E-mail: jean-yves.lapointe@umontreal.ca.

0006-3495/07/01/461/12 $2.00

doi: 10.1529/biophysj.106.092296

penicillin, and 0.1 mg/ml streptomycin for 4–7 days before electrophysiological experimentation.

Molecular biology

The constructions prepared for obtaining the mutants C255A and C511A have been described elsewhere (26).

Electrophysiology

The saline solution normally used in our electrophysiological experiments is composed of (in mM): 90 NaCl, 3 KCl, 0.82 $MgCl_2$, 0.74 $CaCl_2$, and 10 Hepes and the pH was adjusted to 7.6 with NaOH. Two-electrode voltage-clamp experiments were performed using an Oocyte Clamp OC-725 (Warner Instruments, Hamden, CT) and a data acquisition system (Digidata 1322A and Clampex 8.2, Axon Instruments, Union City, CA). Current and voltage microelectrodes were filled with 1 M KCl and had a resistance of 1–2 MΩ. The bath current electrode was an Ag-AgCl pellet, and the reference electrode was a 1 M KCl agar bridge. The oocytes were clamped to a membrane potential (V_m) of −50 mV, and three repetitions of V_m steps between +70 and −170 mV (by increments of 20 mV, 300 ms duration, no series resistance compensation used) were applied with an interval of 1.7 s between each step. Ninety-five percent of the command voltage step was reached in 3–4 ms. Data were obtained with a sampling frequency of 10 kHz, without filtering, and the three repetitions were averaged for each experiment.

Data analysis

Pre-steady-state current analysis was performed as described previously (26). Briefly, the transferred charge was obtained at each membrane potential (Q-V curve) by subtracting the integrated baseline-corrected currents in Pz solution (200 μM) from similar currents in saline solution (either in the presence or absence of αMG). Thus, the transferred charge calculated corresponds to the total charge in one experimental condition minus the total charge in the presence of Pz. The total charge in the presence of Pz was found to be linear with voltage as expected if it was mainly due to the presence of the oocyte capacitive current. The baseline correction was obtained from the mean current measured between 50 and 80 ms after the initiation of a voltage pulse. A simple Boltzmann equation was fitted to the Q-V curve to estimate $V_{1/2}$ (the voltage at which half of the charge is transferred), Q_{max} (the amplitude of the total charge transferred), and z (the valence of the transferred charge) (26). The time constants (τ_{slow}) were evaluated by fitting a double exponential on the $I_{transit}$ ($I_{saline} - I_{Pz}$) with the Clampfit 8.2 program (Axon Instruments). Only the slow time constant (τ_{slow}; 2–10 ms), which has the dominant amplitude, was considered.

Statistics

Experiments were performed on at least six oocytes obtained from a minimum of two different donors. Data are reported as means ± SE and are compared using unpaired Student's t-test; statistical significance was set at $P < 0.05$. Errors bars were omitted when smaller than the symbol size.

RESULTS

Pre-steady-state currents in the presence of αMG for C255A and C511A

In contrast to wt SGLT1, the mutants C255A and C511A clearly exhibit pre-steady-state currents in the presence of a saturating α-methyl-glucose (αMG) concentration (26), particularly at depolarizing V_m levels. Figs. 1 *A* and 2 *A* show the Pz-sensitive currents with different voltage steps for the two mutant proteins using several αMG concentrations (0, 1, 5, and 10 mM αMG). As the capacitive currents are eliminated by subtraction of currents measured in the presence of Pz, the transient currents at each voltage step directly represent SGLT1-specific pre-steady-state currents. The integrals of the transient currents measured at different V_m are used to produce transferred charge versus V_m (Q-V) curves. The Q-V curves for the two mutants are shown in Figs. 1 *B* and 2 *B*. As the cotransporter conformation at very positive V_m levels is predicted to be independent of the presence of extracellular αMG (the binding site being predicted to face inside in all cases (2,4,10)), each Q-V curve was shifted vertically to have $Q = 0$ at +50 mV under all conditions. This allows direct comparison of the transferred charge at different V_m; it is clear that they decrease as the αMG concentration increases. It is also clear from Figs. 1 *B* and 2 *B* that the voltage range over which charge can be transferred is reduced in amplitude and displaced toward more positive potentials when the αMG concentration is increased. The measured charge, at saturating αMG concentration, has reached its plateau level at −50 mV and remains basically constant as V_m becomes more negative. However, a saturating αMG concentration does not totally abolish the transferred charge. A Boltzmann relation can be fitted to the Q-V curves, which yields a value for the parameter $V_{1/2}$, the V_m at which half of the mobile charge is equally balanced between the inward and outward facing positions. For both mutants, an increase in αMG concentration shifts the $V_{1/2}$ toward more positive values. For mutant C255A, the measured $V_{1/2}$ averaged -35 ± 5 mV at 0 mM and 5 ± 5 mV at 10 mM αMG ($n = 6$). For mutant C511A, the corresponding values were -28 ± 2 mV at 0 mM and 13 ± 3 mV at 10 mM αMG ($n = 6$).

The progressive addition of extracellular αMG also affected the τ_{slow} for pre-steady-state currents as depicted in Figs. 1 *C* and 2 *C*. They were obtained by fitting double exponentials to the Pz-sensitive currents. As reported previously (26), in the absence of αMG, τ_{slow} for the mutant proteins reached a plateau of 4–5 ms at hyperpolarized V_m, which is about half of the value measured for the wt SGLT1. An increase in αMG concentration clearly produced an increase of τ_{slow} at positive V_m. For V_m more negative than −50 mV, addition of αMG accelerated the transient currents, as shown in Fig. 2 *C* for 1 mM αMG. The currents in the presence of higher concentrations can no longer be fitted accurately at these voltages (see Fig. 2 *C* for 10 mM αMG and Fig. 1 *C* for 5 and 10 mM αMG). Consequently, at 1 mM αMG, the τ_{slow} versus V_m (τ_{slow}-V) curve has a bell shape centered around −50 mV for both mutants. At 10 mM αMG, τ_{slow} starts at very low values for negative V_m and reaches a value of 6–7 ms for both mutants at depolarizing potentials.

The stability of the preparation as a function of time was tested in each experiment by comparing pre-steady-state currents in the absence of αMG measured before and after

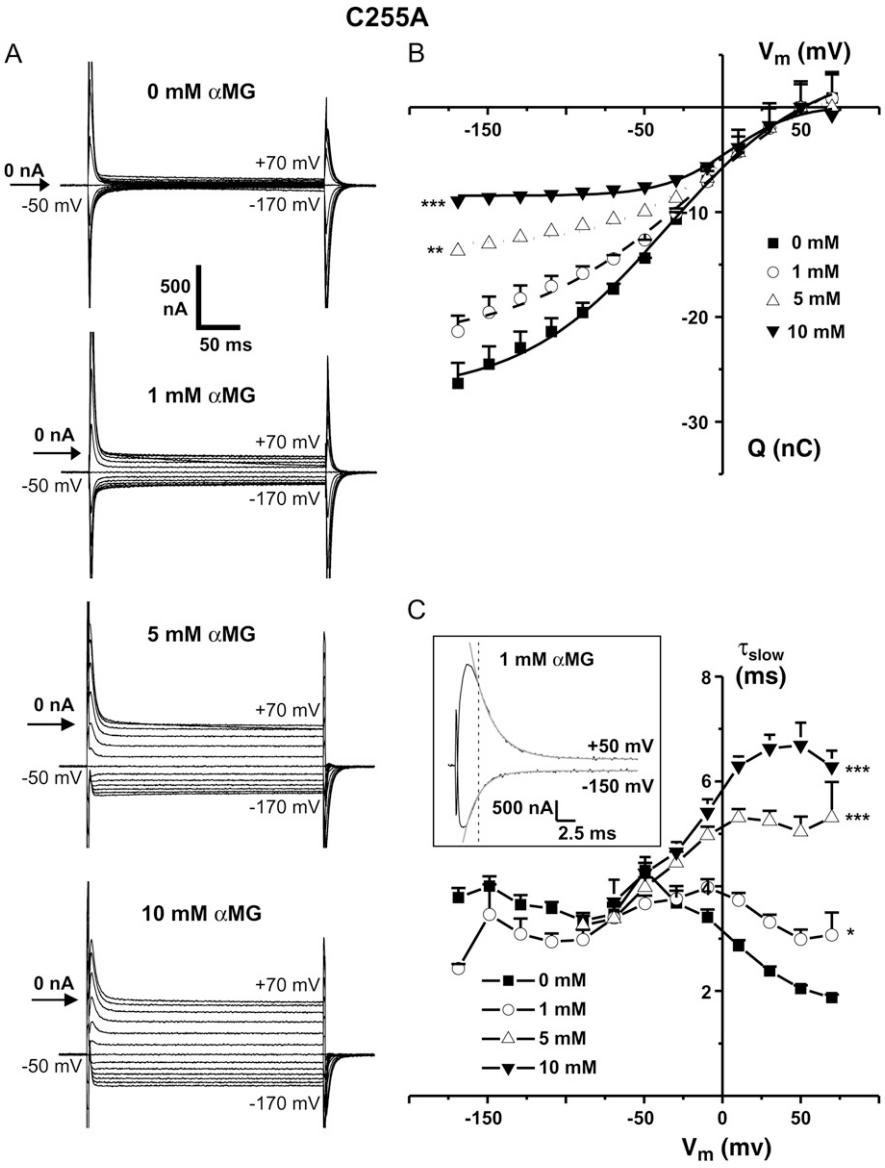

FIGURE 1 Pre-steady-state currents of mutant C255A in the presence of different αMG concentrations. (*A*) Pre-steady-state current traces at different V_m in the presence of various αMG concentrations (0, 1, 5, and 10 mM) for a typical C255A-expressing oocyte. The currents were obtained by subtracting the currents in the presence of 200 μM Pz from the currents measured in the various conditions. (*B*) Q-V curves in different αMG concentrations were compared to those in the absence of substrate. Values were shifted to have the same $Q = 0$ at $V_m = +50$ mV. The curve represents a Boltzmann equation fitted to the points ($n = 6$). (*C*) Time constants of the pre-steady-state currents in different αMG concentrations were compared to those in the absence of substrate ($n = 6$). The inset represents the double exponential fit (*gray line*) of the Pz-sensitive currents (*black line*) shown in panel *A* at 1 mM αMG for the indicated V_m. The dotted line indicates the time at which 95% of the V_m is achieved. Means ± SE are shown. Stars indicate statistical significance with respect to the values in 0 mM αMG (*, $P \leq 0.05$; **, $P \leq 0.01$;***, $P \leq 0.001$).

having presented the different αMG concentrations. In all cases, the Q-V and τ_{slow}-V curves were found identical. In addition, the effects of αMG on the pre-steady-state currents were found to be independent on the order of the αMG conntrations applied (increasing or decreasing concentrations).

Pre-steady-state currents in the presence of αMG for wt SGLT1

Although the inhibitory effect of αMG on wt SGLT1 pre-steady-state currents has long been known (11,25), to our knowledge it has never been studied quantitatively in a dose-dependent manner nor has it been explained with the use of a kinetic model. Given our findings with the two SGLT1 mutant proteins, we sought to characterize this effect in detail on wt SGLT1 and to compare it with that observed for the mutants. Fig. 3 *A* shows Pz-sensitive pre-steady-state currents recorded from wt SGLT1 in the absence or in the presence of different αMG concentrations (0.5 mM, 1 mM, and 5 mM). In agreement with previous reports, addition of extracellular αMG leads to a progressive decrease in the pre-steady-state currents and to the appearance of steady-state inward Na^+/glucose flux, which have been described in detail (11,25). The Q-V curves obtained with different αMG concentrations is illustrated in Fig. 3 *B*. It is obvious that a saturating concentration of αMG (5 mM) completely abolished charge transfer ($n = 9$), at least within the time resolution provided by the two-electrode voltage-clamp technique. In the presence of 5 mM αMG, the amplitude of the transferred charge that can be detected is approximately equal to that measured from a noninjected oocyte (<1 nC). The time constants of these pre-steady-state currents are shown in Fig. 3 *C*. Increased αMG concentrations produce a clear acceleration of the transient currents at negative V_m, whereas the value of the time constant remains

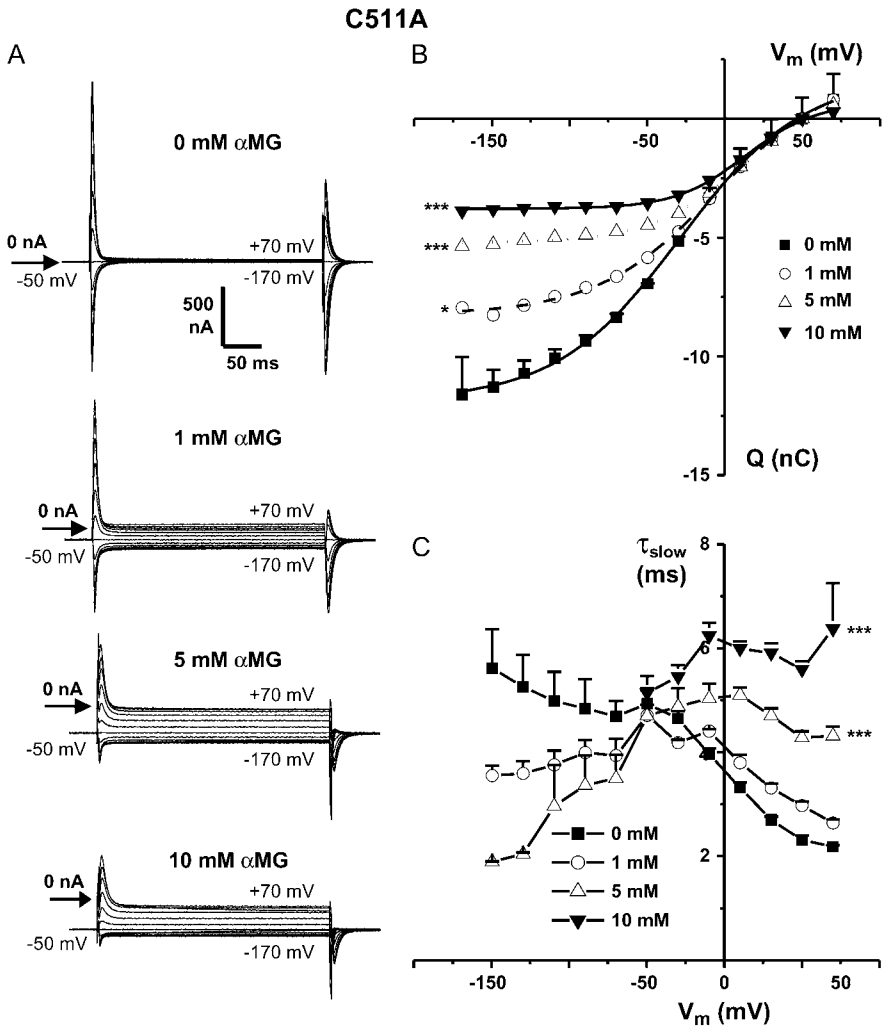

FIGURE 2 Pre-steady-state currents of mutant C511A in the presence of different αMG concentrations. (*A*) Pre-steady-state current traces at different V_m in the presence of various αMG concentrations (0, 1, 5, and 10 mM) for a typical C511A-expressing oocyte. The currents were obtained by subtracting the currents in the presence of 200 μM Pz from the currents measured in the various conditions. (*B*) Q-V curves in different αMG concentrations were compared to those in the absence of substrate. Values were shifted to have the same $Q = 0$ at $V_m = +50$ mV. The curve represents a Boltzmann equation fitted to the points ($n = 6$). (*C*) Time constants of the pre-steady-state currents in different αMG concentrations were compared to those in the absence of substrate. ($n = 6$). Means $\pm$ SE are shown. Stars indicate statistical significance (see Fig. 1 legend).

the same at positive V_m. In the presence of 5 mM αMG, the transient currents are difficult to fit to a double exponential equation because τ_{slow} shows only modest voltage dependence and reaches a value of ~2.5 ms (at +70 mV) with very small amplitude ($n = 7$). Both parameters are close to the limits inherent to the two-electrode voltage-clamp technique.

Fig. 4 summarizes the effects of αMG on the $V_{1/2}$ and on the normalized amplitude of the total transferred charge for wt SGLT1 versus the two mutants. In Fig. 4 *A*, the shift in $V_{1/2}$ produced by the addition of αMG to the wt SGLT1 is compared with the shifts mentioned above for the two mutants. For wt SGLT1, $V_{1/2}$ goes rapidly from -60 ± 5 mV at 0 mM to 12 ± 12 mV at 1 mM αMG ($n = 9$) and, at αMG concentrations higher than 1 mM, the amplitude of the Q-V curve is reduced to such an extent that the fitting of a Boltzmann curve is not reliable. In all cases, the $V_{1/2}$ is progressively shifted toward positive V_m levels as the external [αMG] increases, but this shift is less marked for the mutants than for wt SGLT1.

To quantitatively compare the sensitivity of the pre-steady-state currents to αMG, the decreases in transferred charge caused by αMG were normalized to the total transferred charge in the absence of substrate (i.e., $(Q_{saline} - Q_{\alpha MG})/Q_{saline}$). A simple Michaelis-Menten equation was fitted to $(Q_{saline} - Q_{\alpha MG})/Q_{saline}$ taken at -170 mV as a function of αMG concentration after setting $Q = 0$ for $V_m = +50$ mV (as done in Figs. 1 *B*, 2 *B*, and 3 *B*). It is clear that for the wt SGLT1, a high αMG concentration inhibits 100% of the transferred charge, whereas only partial inhibition (~65–75% inhibition) was observed for the mutant proteins. It was found that the αMG-sensitive charge is consistent with αMG affinity constants ($K_{mQ}^{\alpha MG}$) of 0.48 $\pm$ 0.05 mM for wt SGLT1 (see Fig. 4 *B*), 5 $\pm$ 2 mM for mutant C255A, and 2 $\pm$ 1 mM for mutant C511A whereas their $K_{mI}^{\alpha MG}$ constants, using αMG-sensitive cotransport current (steady-state values, $I_{ss}(\alpha MG)$), were 0.97 $\pm$ 0.1 mM for wt SGLT1 (26,27), 1.6 $\pm$ 0.2 mM (C255A), and 1.6 $\pm$ 0.2 mM (C511A) at -170 mV (26).

Kinetic model for pre-steady-state currents

A scheme of the simple five-state kinetic model used is presented in Fig. 5. The substrate-binding and -debinding

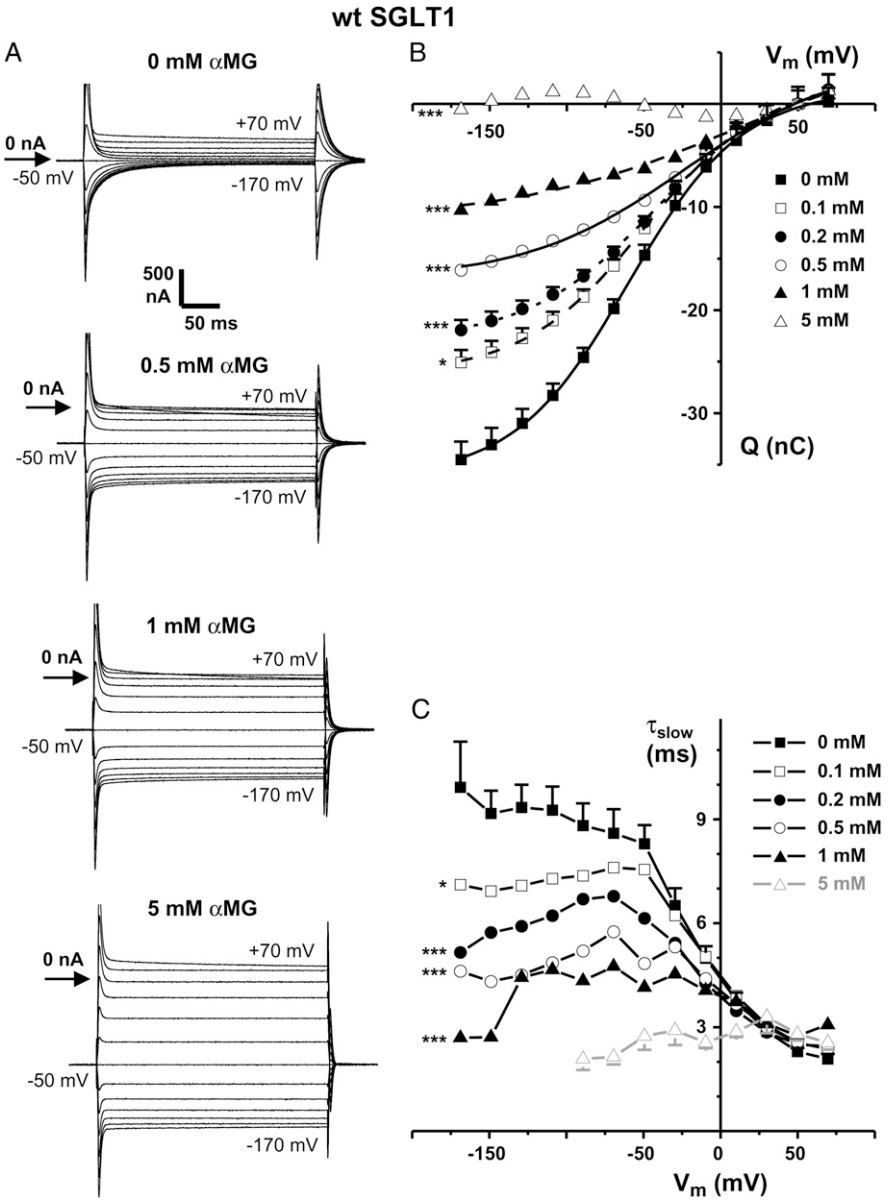

FIGURE 3 Pre-steady-state currents of wt SGLT1 in the presence of different αMG concentrations. (*A*) Pre-steady-state current traces for different V_m in the presence of various αMG concentrations (0, 0.5, 1, and 5 mM) containing solutions for a typical wt SGLT1-expressing oocyte. The currents were obtained by subtracting the currents in the presence of 200 μM Pz to the ones in the various conditions. (*B*) Q-V curves in different αMG concentrations as compared to those in the absence of substrate. Values were shifted to have the same $Q = 0$ at $V_m = +50$ mV. The curve represents a Boltzmann relation fitted to the points ($n = 9$). (*C*) Time constants of the pre-steady-state currents in different αMG concentrations as compared to those in the absence of substrate. The time constants at 5 mM αMG were plotted in gray because of the small amplitude of the exponential giving uncertainty about the value of this time constant ($n = 7$). Means ± SE are shown. Stars indicate the statistical significance (see Fig. 1 legend).

steps (k_{45} and k_{54}) are voltage independent (2,28) as are the lumped reactions k_{41} and k_{51}, which represent the conformational changes of the Na^+-loaded transporter (involved in the leak current) and the Na^+- and αMG-loaded transporter, respectively, with their associated intracellular release steps. It was found that the extracellular Na^+-binding reaction could be assumed to be a fast reaction at equilibrium without losing any fitting performance. The voltage-dependent reactions are expressed as follows (for $i = 1, 2, 3$; $j = i + 1$):

$$k_{ij} = k_{ij0}\exp\left(z_i\alpha_i\frac{FV_m}{RT}\right),\ k_{ji} = k_{ji0}\exp\left(-z_i(1-\alpha_i)\frac{FV_m}{RT}\right), \quad (1)$$

where z_i is the valence of the equivalent moving charge, α_i represents the asymmetry of the energy barrier, V_m is the membrane potential, and F, R, and T have their usual meanings (see also Table 1).

The affinity for intracellular Na^+ (K_m^{Na+}) was previously estimated for rabbit SGLT1 in giant, excised, inside-out patches and was found to vary from 44 to 70 mM (28,29). In agreement with these estimates, we recently found that intracellular Na^+ has to be increased by blocking the Na^+/K^+-ATPase overnight to generate a measurable outward Na^+/glucose current upon intracellular glucose injection (30). This is consistent with an intracellular K_m^{Na+} much higher than the physiological intracellular Na^+ concentration. On the other hand, the estimation of $K_m^{\alpha MG}$ for the intracellular site is ~35 mM (28,29). Consequently, under physiological conditions, the inverse mode of transport is highly unlikely, which is reflected by very low values of k_{14} and k_{15} (see

Table 1). Thus, we assumed that the probability of finding the intracellular site loaded with Na^+ and αMG was negligible, and we reduced the potential seven-state kinetic model into the five-state kinetic model shown in Fig. 5.

The numerical simulations were performed using MATLAB 6.5.0 software (MathWorks, Natick, MA). Transferred charges were calculated as the integral of the pre-steady-state currents as done during the analysis of the experimental data and were also fitted with a simple Boltzmann curve to deduce the $V_{1/2}$, Q_{max}, and z parameters. As the analytical expression for the time constant in the presence of substrate cannot be obtained in a five-state model, the numerical values of the time constant were obtained by taking the reciprocal of the eigenvalues of the following matrix, as previously reported (10):

$$\frac{d}{dt}\begin{bmatrix} C_1 \\ C_2 \\ C_3 \\ C_4 \\ C_5 \end{bmatrix} = \begin{bmatrix} -(k_{12}+k_{15}) & k_{21} & 0 & 0 & k_{51} \\ k_{12} & -(k_{21}+k_{23}) & k_{32} & 0 & 0 \\ 0 & k_{23} & -(k_{32}+k_{34}) & k_{43} & 0 \\ k_{14} & 0 & k_{34} & -(k_{45}+k_{43}+k_{41}) & k_{54} \\ k_{15} & 0 & 0 & k_{45} & -(k_{54}+k_{51}) \end{bmatrix} \begin{bmatrix} C_1 \\ C_2 \\ C_3 \\ C_4 \\ C_5 \end{bmatrix}.$$

Moreover, the model predicts the relaxation of pre-steady-state currents toward steady-state currents. The current (I) versus V_m curves are sigmoid, as observed for the experimental current versus membrane potential (I-V) curves in the absence and in the presence of αMG (not shown). The rate constants of the model were adjusted by trial and error to obtain a satisfactory fit to the measured Q-V curves, the $V_{1/2}$, and the τ_{slow}s of the pre-steady-state currents. The steady-state parameters (I-V curves, K_m^{Na+}, or $K_m^{\alpha MG}$) were not considered as criteria for the adjustment of the model parameters but were found afterwards to be in accordance with the experimental values.

Simulation of pre-steady-state currents in the absence of αMG

Table 1 gives the rate constants used by Chen et al. (4) and by Loo et al. (11) as well as the rate constants used by this study to simulate the time constants of the pre-steady-state currents. As shown in Fig. 6 *A*, our new set of rate constants can reproduce, in a generally satisfying manner, the currents, the Q-V curves, and the τ_{slow}-V curves for wt SGLT1 exposed to different αMG concentrations. In the presence of 90 mM Na^+, a k_{210}/k_{120} ratio of ~0.5 is required for the plateau effect seen on the τ_{slow}-V curve at hyperpolarizing V_m. k_{23} is a crucial rate constant because it is voltage independent and becomes rate limiting for V_m below −70 mV (at 90 mM Na^+). Indeed, the value of $1/k_{23}$ closely corresponds to the plateau value reached by τ_{slow} at very negative V_m. The ratio k_{23}/k_{32} is also responsible for the voltage dependence of τ_{slow} observed at depolarizing V_m. At 0 mV, K_{34} (the ratio k_{43}/k_{34}) is 0.1 M^2 for wt SGLT1 and 0.07 M^2 for the mutants and is largely responsible for the Na^+ affinity measured at low αMG concentration. This ratio also has a large influence on the position of the $V_{1/2}$ of the Q-V curve. The K_{34} and the k_{23} values were modified for simulation of transferred charges through the mutant proteins to account for the faster τ_{slow} at negative V_m and the new $V_{1/2}$ of −30 mV (instead of −50 mV), which was observed for both mutants (26). These two simple modifications yielded the fit for the Q-V curve of Fig. 6 *B* (*left panel*), shown for mutant C511A, and the τ_{slow}-V curve shown in Fig. 6 *B* (*right panel*) at 5 mM αMG.

Simulation of the effect of αMG on the pre-steady-state currents

To interpret the effects of αMG on the pre-steady-state currents, appropriate values for the parameters k_{45}, k_{54}, and k_{51} have to be determined. Our strategy was to start by establishing parameters that could explain the behavior of the transferred charges of wt SGLT1 in the presence of different αMG concentrations. Our first criterion was that the transferred charge had to disappear in the presence of a saturating αMG concentration. The k_{ij} of the four-state model established in the absence of αMG were maintained constant, and we investigated the effects of the three new k_{ij} on the simulated Q-V curve. We started with the parameters proposed by Loo et al. (11) (see Table 1) but needed to increase the value of k_{51} by up to 40-fold over the original value (2000 vs. 50 s^{-1}) to reproduce the charge disappearance observed at high αMG concentration. It was also clear that the ratio k_{45}/k_{54} influenced the $V_{1/2}$ of the Q-V curve: an increase in this ratio shifts the $V_{1/2}$ toward more positive V_m. However, the absolute values of k_{45} and k_{54} (and not only their ratio) were also important in the global behavior of the Q-V curve as a function of αMG concentration. With respect to the values proposed by Loo et al. (11), the values of k_{45} and k_{54} had to be increased by factors of 30 and 50, respectively.

For the mutants, we first established the values of the parameters k_{210}, k_{23}, and K_{340} to account for the faster time constants and the positive shift in $V_{1/2}$ in the absence of αMG. Changes in k_{210} and k_{23} were necessary along with more modest

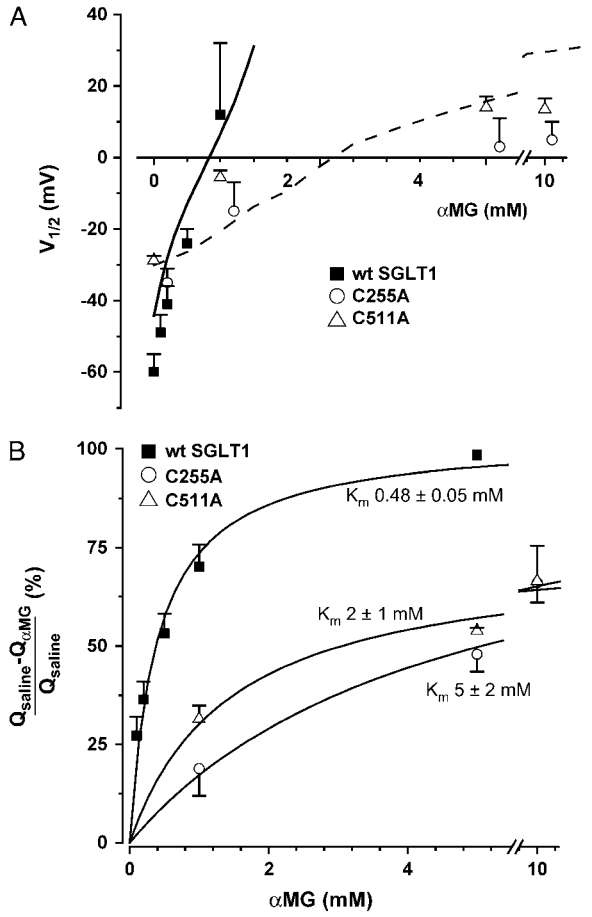

FIGURE 4 Effect of αMG on $V_{1/2}$ and estimation of $K_{mQ}^{\alpha MG}$ with the transferred charge. (*A*) $V_{1/2}$ of C255A (*open circles*), C511A (*open triangles*), and wt SGLT1 (*solid squares*) in the presence or absence of different αMG concentrations. The lines represent the extracted $V_{1/2}$ values from the theoretical Q-V curves obtained with the kinetic model's current simulations (*solid line*: wt SGLT1, *dotted line*: mutants). The phenomenological parameter $V_{1/2}$ is obtained by a simple Boltzmann relation fitted to the experimental and theoretical Q-V curves (see Figs. 1 *B*, 2 *B*, and 3 *B*). (*B*) Normalized αMG-dependent transferred charge in the presence of different αMG concentrations $((Q_{saline} - Q_{\alpha MG})/Q_{saline})$ of wt SGLT1 (*solid square*), C255A (*open circle*), and C511A (*open triangle*) at −170 mV. The line represents a simple Michaelis-Menten equation fitted to the points, and the corresponding K_m value from the fit is noted. Means ± SE are shown.

changes in the remaining parameters describing the αMG-independent steps of the kinetic model. The new values of k_{45}, k_{54}, and k_{51} found for the wt transporter could not reproduce the observed Q-V and τ_{slow}-V curves of the mutants. We found that the reactions describing αMG binding and debinding had to be reduced by an order of magnitude and the reorientation of the fully loaded carrier (k_{51}) had to be massively decreased from 2000 to 80 s^{-1}. The best parameter set found is presented in Table 1 for wt SGLT1 and the mutants.

Simulations of wt SGLT1

The simulated wt SGLT1 Q-V curves are shown in Fig. 6 *A* (*middle panel*), superimposed on the experimental data

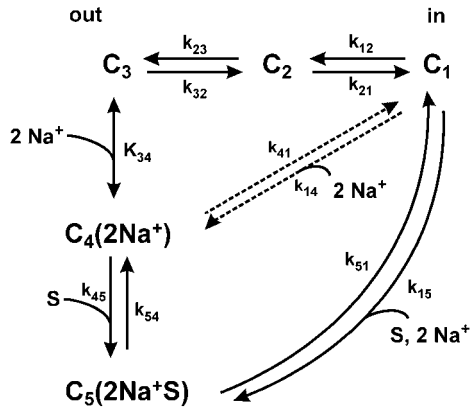

FIGURE 5 Kinetic model of the SGLT1 for the estimation of pre-steady-state currents. The voltage-independent substrate-binding/debinding events are included (k_{45}, k_{54}) in contrast to the models previously described in Chen et al. (4) and in Gagnon et al. (26). See Table 1 for rate constant values and Results and Discussion for further details.

points (in *gray*). Although, the shapes of the theoretical and experimental Q-V curves differ slightly, the general decrease due to external αMG concentration is well represented. Three parameters were used to measure the accuracy of the model predictions: the $V_{1/2}$ of the Q-V curves, the normalized transferred charge curves in the presence of different αMG concentrations $((Q_{saline} - Q_{\alpha MG})/Q_{saline})$, as well as the τ_{slow}-V curve. Fig. 4 *A* illustrates the phenomenological parameter $V_{1/2}$ as a function of αMG concentration extracted from the fits of a simple Boltzmann relation to our theoretical Q-V curves (*solid line*). Although the theoretical Q-V curve differs slightly from a simple Boltzmann relation, the model correctly represents the voltage shift produced by αMG addition. The model also correctly predicts the total inhibition of the transferred charge by a saturating αMG concentration. We estimated an apparent affinity for αMG ($K_{mQ}^{\alpha MG}$), using the remaining charge in the presence of αMG $((Q_{saline} - Q_{\alpha MG})/Q_{saline})$, to compare it with that obtained experimentally. The parameters given in Table 1 yield a $K_{mQ}^{\alpha MG}$ value of 0.40 ± 0.07 mM at −170 mV, which is not significantly different from the experimental value reported above. Finally, Fig. 6 *A* (*right panel*) shows that the τ_{slow}-V curve values are close to the experimental values as the model reproduces very well the acceleration of the transient currents at hyperpolarizing V_m and shows the bell-shaped curve peak shifting toward more positive V_m as the αMG concentration increases.

Simulations of the mutant SGLT1s

The simulated Q-V curves for the mutant SGLT1s are shown in Fig. 6 *B* (*middle panel*), superimposed on the experimental data points for mutant C511A alone (in *gray*) because mutant C255A produced very similar values. The charge plateau value reached at hyperpolarizing V_m, at 5 and 10 mM αMG, is reproduced very well by the modeled Q-V curve. The dotted line on Fig. 4 *A* illustrates $V_{1/2}$ as a function of αMG

TABLE 1 Rate constants of a five-state kinetic model used for the pre-steady-state current simulations of wt SGLT1 and mutants

	k_{120}* (s^{-1})	k_{210} (s^{-1})	k_{23} (s^{-1})	k_{320} (s^{-1})	K_{340}† (M^2)	k_{41}‡ (s^{-1})	k_{45} ($M^{-1}s^{-1}$)	k_{54} (s^{-1})	k_{51}‡ (s^{-1})
Loo et al. (11)§	25	600	–	–	0.021	0.3	10,000	20	50
Chen et al. (4)	790	370	100	280	0.153	–	–	–	–
wt SGLT1	790	370	110	130	0.1	10	300,000	1000	2000
Mutants	790	230	230	100	0.072	10	60,000	100	80

*The constants k_{ij0} represent the value of k_{ij} at 0 mV (see Eq. 1). The rate constants that are independent of V_m are simply noted k_{ij}. The values of z_i used for the equivalent charge moving across the entire membrane electrical field in the step between state "i" and "$i + 1$" were −0.38, −0.52, and −1.1 for i varying from 1 to 3, respectively. The values for α_i describing the asymmetry of the energy barrier were 0.3 and 0 for i of 1 and 2, respectively.

†The Na^+-binding step is assumed to be in rapid equilibrium. K_{340} represents the ratio k_{430}/k_{340}, the equilibrium dissociation constant. This simplification eliminates the need for α_3 in the description of the voltage-dependent Na^+-binding step.

‡The constants k_{14} (in $M^{-2}s^{-1}$) and k_{15} (in $M^{-3}s^{-1}$) were calculated to respect microreversibility. If the intracellular Na^+ concentration is set at 7 mM, the reaction rates from state 1 to state 4 are 0.009 s^{-1} and 0.05 s^{-1} for wt SGLT1 and for the mutants, respectively. If the intracellular αMG concentration is 0.1 mM, the reaction rates from state 1 to state 5 are 0.05 s^{-1} and 0.03 s^{-1} for wt SGLT1 and for the mutants, respectively.

§In the model of Loo et al. (2,11), there are six states and no intermediate state between our C_1 and C_3. Moreover, there are two additional states representing the intracellular facing fully loaded transporter and Na^+-loaded transporter, which are lumped into k_{41} and k_{51} in our model. See Results and Discussion for more details and references.

concentration for the mutants. It is clear that the estimated $V_{1/2}$ for the modeled Q-V curves of the mutants closely reproduced the characteristics of both mutants. The model accounts for the partial inhibition of the transferred charge at high αMG concentrations. In addition, the $K_{mQ}^{\alpha MG}$ was estimated with the remaining charge in the presence of αMG $((Q_{saline} - Q_{\alpha MG})/Q_{saline})$ and provided the value of 4 ± 2 mM at −170 mV, which is close to the experimental values reported above for C255A and, to a lesser extent, for C511A (5 ± 2 mM and 2 ± 1 mM, respectively). Finally, the theoretical τ_{slow} values were superimposed on the experimental values for both mutants at 5 mM αMG in Fig. 6 *B* (*right panel*). The model predicts two exponentials with significant amplitudes with time constants in the range of 2–6 ms in the presence of αMG. The first one is almost identical with that observed in the absence of αMG. The second one is slower at depolarizing V_m where it reaches a plateau value of ~5.5 ms. Experimentally, a single exponential with a time constant in the millisecond range could be detected. Given the limited speed of the voltage pulse, the typical noise level found in our current recording, and given

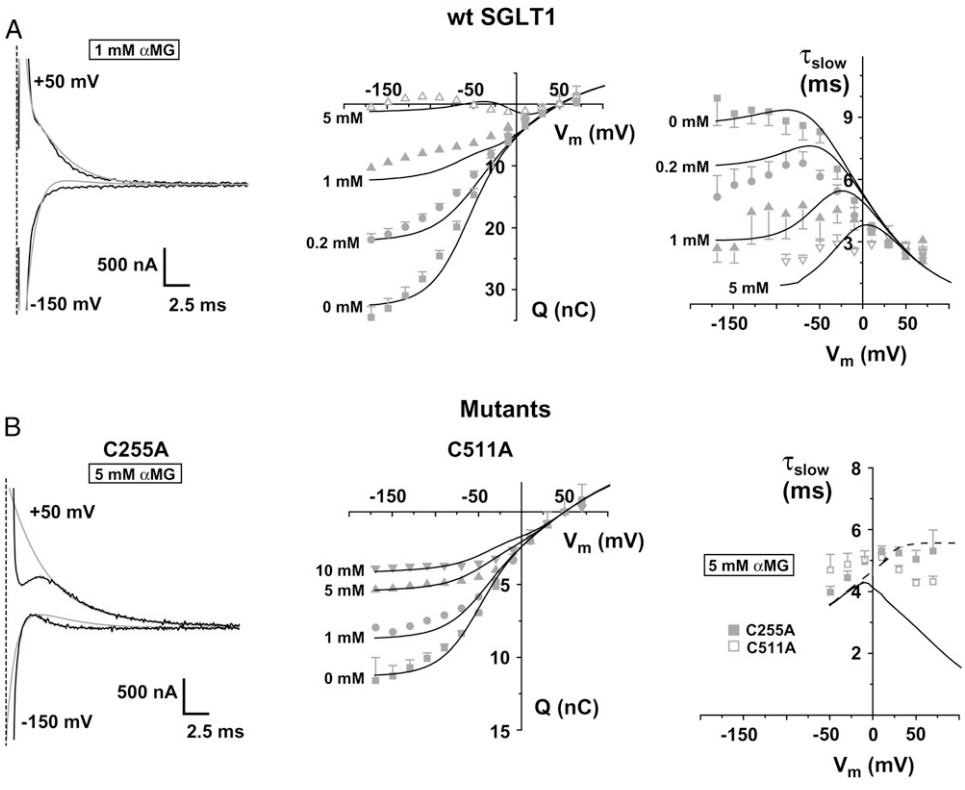

FIGURE 6 Predictions of the kinetic model. (*A*) Predictions of the kinetic model superimposed on the experimental data for wt SGLT1. The left panel shows simulated currents (*gray line*) superimposed on the experimental current (*black line*) at 1 mM αMG for the indicated V_m; the vertical dotted line indicates the beginning of the voltage step. The middle panel illustrates the Q-V curves, and the right panel shows τ_{slow} as a function of V_m at different αMG concentrations. (*B*) Predictions of the kinetic model superimposed on the experimental data for mutants. The left panel shows the experimental current (*black line*) of mutant C255A superimposed on the simulated currents at 1 mM αMG (*gray line*) for the indicated V_m; the vertical dotted line indicates the beginning of the voltage step. The middle panel illustrates the Q-V curves for mutant C511A, and the right panel shows τ_{slow} as a function of V_m for both mutants at 5 mM αMG. The currents from wt SGLT1 and C255A come from the experiment presented in Figs. 3 *A* and 1 *A*, respectively. The experimental data points were represented in gray for comparison. For clarity, only data points from mutant C511A are presented for the Q-V curve. The Q-V curve was shifted vertically such that $Q = 0$ at +50 mV. As the model predicts significant amplitudes for two exponential components, the two time constants (a fast one, *solid line*, and a slower one, *dashed line*) are presented.

the fact that the two predicted time constants are in the same order of magnitude, it is conceivable that our experimental time constant would correspond to some intermediate value between the predicted ones. Thus it is concluded that the model reproduces fairly well the experimental time constants measured in the presence of αMG.

DISCUSSION

The identification of a disulfide bridge between C255 and C511 constitutes an important step in our understanding of how the 14 transmembrane segments are located with respect to each other and in the eventual identification of the physical structure that serves as the ''voltage sensor'' in SGLT1 (26). The two mutants C255A and C511A were found to display further interesting features which confirmed the importance of this region of the cotransporter. In this study we report that, in contrast with wt SGLT1, these two mutants exhibit pre-steady-state currents in the presence of a saturating αMG concentration. By analyzing the dose-dependent effects of αMG on the pre-steady-state currents of these mutants as well as for wt SGLT1, we sought to identify a satisfying kinetic explanation for both the partial diminution of mutant pre-steady-state currents by αMG and for the complete disappearance of the wt SGLT1 transient currents.

The pre-steady-state currents in the absence of αMG have been studied using cut open oocytes exposed to various Na^+ concentrations, and a simple four-state kinetic model (4) was found to be consistent with the amplitudes and the time constants (τ_{fast} (<1 ms) and τ_{slow} (1–10 ms)) of the experimentally determined pre-steady-state currents as a function of the external Na^+ concentration. The presence of these two time constants was more recently confirmed for rabbit SGLT1 (7,8) and for hSGLT1 (10). In this last study, fluorescently labeled cotransporters were also used and a slower time constant of ~100 ms was reported in addition to τ_{fast} and τ_{slow}. A seven-state model was suggested for the translocation of the free transporter and the binding of two external Na^+ ions, but the authors could not find a parameter set that would be in quantitative agreement with their own observations. Considering the time resolution provided by the two-electrode voltage-clamp technique, we decided to use the four-state model proposed by Chen et al. (4) to explain the effects of disrupting the disulfide bridge C255-C511 on the $V_{1/2}$ of the Q-V and τ_{slow}-V curves in the absence of αMG (26). In the original model, it was assumed that a single Na^+ ion was involved in the pre-steady-state currents. To incorporate αMG binding, and given that the cotransport stoichiometry is 2 Na^+:1 glucose (31), we simply replaced the original rate constant for Na^+ binding (k_{34}) by $k_{34}/[Na^+]$ to account for both Na^+ ions and made it a second order rate constant in $M^{-2}s^{-1}$. As the extracellular Na^+ concentration is constant in this study, further studies will have to test whether the model used is consistent with the effects of changes in external Na^+ concentration.

Occupancy probabilities in the presence and absence of αMG

In the absence of αMG and at −50 mV, the set of rate constants proposed in Table 1 leads to occupancy probabilities (C_i) of 5%, 22%, 43%, and 30% (from $i = 1$ to 4), indicating that 73% of the Na^+-binding sites are exposed outside either in a free or Na^+-bound state (4,26). Obviously this situation is highly voltage dependent and, at +70 mV, C_1 and C_2 now represent 52% and 40% of the cotransporter conformations, respectively. If, from state C_4 to state C_1, the total number of unitary charges that can move across the entire membrane electrical field is 2 ($|z_1 + z_2 + z_3| = 2$), the occupancy probabilities at +70 mV indicate that all but 11% of it has already moved into the inward facing configuration. Fig. 7 *A* presents the occupancy probabilities in the absence of αMG for an extreme voltage step from +70 to −150 mV. Upon hyperpolarization, C_1 rapidly transforms into C_2 and the free binding sites exposed to the extracellular solution (C_3) become Na^+-bound immediately. The step $C_1 \rightarrow C_2$ is considered to be mainly responsible for the fast component to the transient current. In contrast, the following slow transformation of C_2 into C_3 (which is in equilibrium with $C_4(2Na^+)$) is clearly responsible for the slow component of the observed transient currents. Fig. 7, *B* and *C*, presents the changes in occupancy probability for a similar voltage step but in the presence of αMG at 1 or 5 mM. At +70 mV, the starting probabilities are independent of the presence of αMG in the extracellular solution as are the fast events occurring in the first millisecond after hyperpolarization. At −150 mV, the slowest rate constant in the reactions leading to the inward Na^+/glucose current is clearly k_{23}. This is why C_2 accumulates transiently (75%) then relaxes to a value consistent with the steady-state cotransport rate allowed by the external αMG concentration. This is shown in Fig. 7 *D* where the probability of finding C_2 is plotted as a function of time for different αMG concentrations.

For the mutants, the rate constants of Table 1 lead to occupancy probabilities of 2%, 9%, 45%, and 44% (from $i =$ 1 to 4) at −50 mV in the absence of αMG, which is quite similar to the C_i probabilities found for wt SGLT1. At +70 mV, the distribution is slightly different from the wt SGLT1 as C_2 now dominates with a probability of 42% with respect to C_1 (34%), whereas the outward facing, free binding site (C_3) presents a significant probability of 23%. Fig. 8 *A* presents the changes in C_i as a function of time for an extreme voltage pulse from +70 mV to −150 mV. Once again, in the absence of αMG, C_2 is transiently accumulated before relaxing to <5% as the Na^+-bound form ($C_4(2Na^+)$) progressively rises to more than 90%. Fig. 8, *B* and *C*, depicts the occupancy probabilities in the presence of 1.5 and 5 mM αMG. Under these circumstances, and in marked contrast to wt SGLT1, C_2 continues to relax to a low value and it is $C_5(2Na^+S)$, the fully loaded transporter, that progressively increases and attains up to 48% (this value increases to 58% at 10 mM αMG). As

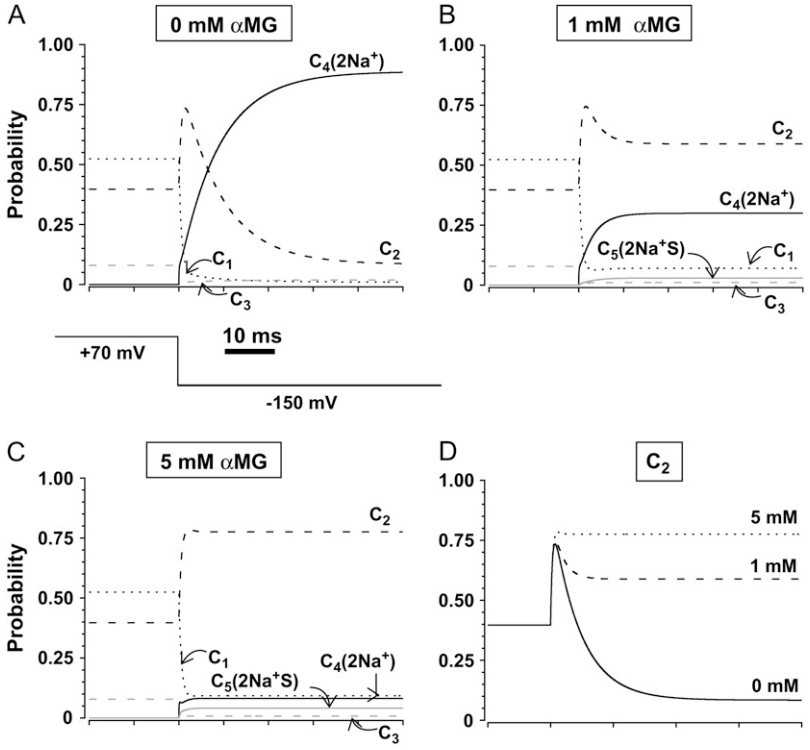

FIGURE 7 Occupancy probability (C_i) as a function of time as calculated by the five-state kinetic model for wt SGLT1. (*A*) Time course of wt SGLT1 occupancy probabilities (90 mM Na^+) for a V_m pulse from +70 mV to −150 mV in the absence of αMG and in the presence of 1 mM αMG (*B*) and 5 mM αMG (*C*). (*D*) Time course of wt SGLT1 C_2 occupancy probability in the absence of αMG (*solid line*, 90 mM Na^+) or in the presence of 1 mM (*dashed line*) or 5 mM (*small dashed line*) αMG for a V_m pulse from +70 mV to −150 mV.

illustrated in Fig. 8 *D*, contrary to what was seen for wt SGLT1, the C_2 state increases (55%) and then relaxes to much lower steady-state values of 5% and 21% in the absence or presence of αMG, respectively. This simply reflects the fact that, for the mutant proteins, the slowest rate constant in the steps mediating Na^+/glucose cotransport at −150 mV is k_{51}. As the steps involved in generating the slow component of pre-steady-state currents are the transition between C_2 and

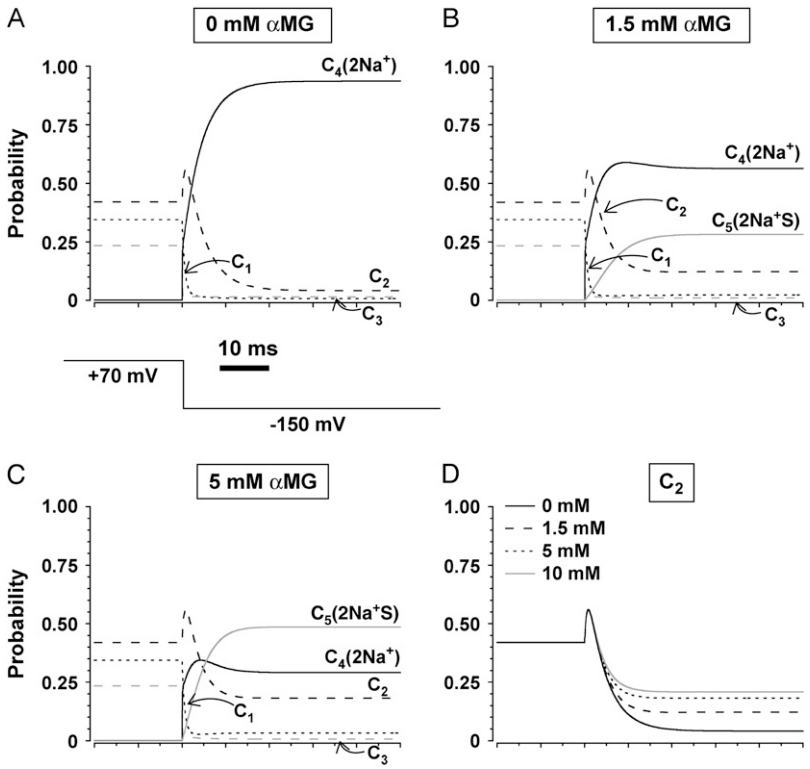

FIGURE 8 Occupancy probability (C_i) as a function of time as calculated by the five-state kinetic model for the mutants. (*A*) Time course of mutant SGLT1 occupancy probabilities (90 mM Na^+) for a V_m pulse from +70 mV to −150 mV in the absence of αMG, in the presence of 1.5 mM αMG (*B*), and in the presence of 5 mM αMG (*C*). (*D*) Time course of mutant C_2 occupancy probability in the absence of αMG (*solid line*, 90 mM Na^+) or in the presence of 1.5 mM (*dashed black line*) or 5 mM (*small dashed black line*) or 10 mM (*solid gray line*) αMG for a V_m pulse from +70 mV to −150 mV.

$C_4(2Na^+)$, Figs. 7 *D* and 8 *D* illustrate the reason transient currents disappear in the presence of αMG for the wt transporter but not for the mutants.

Apparent affinity for αMG

We presented two distinct methods of estimating the apparent affinity for the substrate: one can use the steady-state currents ($I_{ss}(\alpha MG)$) and obtain $K_{mI}^{\alpha mG}$ or the substrate-dependent charge disappearance $((Q_{saline} - Q_{\alpha MG})/Q_{saline})$ to obtain $K_{mQ}^{\alpha mG}$. For the wt SGLT1, both experimental (0.97 and 0.48 mM) and theoretical (0.36 and 0.40 mM) approaches show that the $K_{mI}^{\alpha MG}$ and the $K_{mQ}^{\alpha mG}$ are close in value. However, the two experimental K_m estimates for the mutants are significantly different, particularly for mutant C511A. It is important to specify that these two K_m are apparent K_m and depend not only on the rate constants k_{45} and k_{54} but also on the other rate constants. It seems that the rate-limiting step position is crucial for this discrepancy and that the two methods of obtaining an apparent affinity constant for αMG should be considered with caution. The accordance between their values for wt SGLT1 may simply be coincidental.

Role of the disulfide bridge C255-C511 in SGLT1

In a previous study, we have shown that the breakage of a disulfide bridge between C255 and C511 using dithiothreitol or by disruption through specific alanine mutations led to a displacement of the equilibrium position of the ''voltage sensor'' and to an acceleration of time constant of pre-steady-state current in the absence of αMG (26). In this study, we established that the disulfide bridge C255-C511 (in hSGLT1) also plays a major role in facilitating the conformational change of the fully loaded cotransporter. In addition, a minor role was also detected in the αMG-binding and -debinding reactions. In the absence of a tridimensional structure, it is impossible to know the exact position of this disulfide bridge in relation to the Na^+ or αMG-binding sites, but it is certainly important for the mechanical structure involved in those processes.

CONCLUSIONS

In summary, this study has provided a quantitative explanation for the observation that transient currents disappear in the presence of αMG for the wt SGLT1 but not for the mutant transporters. In wt SGLT1 and in the presence of substrate, the rate-limiting step is from state 2 to state 3. The transferred charges are not observed in this case because, upon hyperpolarization from a very positive to a very negative V_m, the large steady-state current requires a high C_2 probability. Under these circumstances, the steady-state transporter distribution is predicted to simply move from state 1 to state 2, which should generate only a very fast transient current ($\tau \approx$ 0.5 ms). In contrast, for the mutants C255A and C511A in the presence of αMG, the rate-limiting step is from state 5 to state 1. The transporter after having reached a high C_2 probability will relax to a much lower level to reach the required C_5 probability to account for the steady-state current. As the transporter moves from state 2 to states 3–5 through electrogenic steps, a slow transient current is generated. The behavior of the mutants underscores the role played by the rate-limiting step in the possibility of observing pre-steady-state currents. It also reveals the importance of the disulfide bridge C255-C511 in facilitating the translocation of the fully loaded transporter from the outward facing to the inward facing configuration.

We thank Michael Coady for valuable discussions and for his comments on the manuscript.

This work was supported by the Canadian Institutes of Health Research (grant No. MOP-10580). D.G.G. is a Natural Sciences and Engineering Research Council of Canada and Fonds de la recherche en santé du Québec postgraduate scholar.

REFERENCES

1. Hediger, M. A., M. J. Coady, T. S. Ikeda, and E. M. Wright. 1987. Expression cloning and cDNA sequencing of the Na+/glucose cotransporter. *Nature*. 330:379–381.
2. Parent, L., S. Supplisson, D. D. Loo, and E. M. Wright. 1992. Electrogenic properties of the cloned Na+/glucose cotransporter: II. A transport model under nonrapid equilibrium conditions. *J. Membr. Biol.* 125:63–79.
3. Chen, X. Z., M. J. Coady, F. Jalal, B. Wallendorff, and J. Y. Lapointe. 1997. Sodium leak pathway and substrate binding order in the Na+-glucose cotransporter. *Biophys. J.* 73:2503–2510.
4. Chen, X. Z., M. J. Coady, and J. Y. Lapointe. 1996. Fast voltage clamp discloses a new component of presteady-state currents from the Na(+)-glucose cotransporter. *Biophys. J.* 71:2544–2552.
5. Falk, S., A. Guay, C. Chenu, S. D. Patil, and A. Berteloot. 1998. Reduction of an eight-state mechanism of cotransport to a six-state model using a new computer program. *Biophys. J.* 74:816–830.
6. Falk, S., N. Oulianova, and A. Berteloot. 1999. Kinetic mechanisms of inhibitor binding: relevance to the fast-acting slow-binding paradigm. *Biophys. J.* 77:173–188.
7. Krofchick, D., S. A. Huntley, and M. Silverman. 2004. Transition states of the high-affinity rabbit Na(+)/glucose cotransporter SGLT1 as determined from measurement and analysis of voltage-dependent charge movements. *Am. J. Physiol. Cell Physiol.* 287:*C46–C54*.
8. Krofchick, D., and M. Silverman. 2003. Investigating the conformational states of the rabbit Na+/glucose cotransporter. *Biophys. J.* 84:3690–3702.
9. Wright, E. M., and E. Turk. 2004. The sodium/glucose cotransport family SLC5. *Pflugers Arch.* 447:510–518.
10. Loo, D. D., B. A. Hirayama, A. Cha, F. Bezanilla, and E. M. Wright. 2005. Perturbation analysis of the voltage-sensitive conformational changes of the Na+/glucose cotransporter. *J. Gen. Physiol.* 125:13–36.
11. Loo, D. D., A. Hazama, S. Supplisson, E. Turk, and E. M. Wright. 1993. Relaxation kinetics of the Na+/glucose cotransporter. *Proc. Natl. Acad. Sci. USA*. 90:5767–5771.
12. Boorer, K. J., D. D. Loo, and E. M. Wright. 1994. Steady-state and presteady-state kinetics of the H+/hexose cotransporter (STP1) from Arabidopsis thaliana expressed in Xenopus oocytes. *J. Biol. Chem.* 269:20417–20424.
13. Bossi, E., E. Centinaio, M. Castagna, S. Giovannardi, S. Vincenti, V. F. Sacchi, and A. Peres. 1999. Ion binding and permeation through the lepidopteran amino acid transporter KAAT1 expressed in Xenopus oocytes. *J. Physiol.* 515:729–742.

14. Coady, M. J., M. H. Chang, F. M. Charron, C. Plata, B. Wallendorff, J. F. Sah, S. D. Markowitz, M. F. Romero, and J. Y. Lapointe. 2004. The human tumour suppressor gene SLC5A8 expresses a Na+-monocarboxylate cotransporter. *J. Physiol.* 557:719–731.

15. Coady, M. J., B. Wallendorff, D. G. Gagnon, and J. Y. Lapointe. 2002. Identification of a novel Na+/myo-inositol cotransporter. *J. Biol. Chem.* 277:35219–35224.

16. Eskandari, S., D. D. Loo, G. Dai, O. Levy, E. M. Wright, and N. Carrasco. 1997. Thyroid Na+/I- symporter. Mechanism, stoichiometry, and specificity. *J. Biol. Chem.* 272:27230–27238.

17. Fesce, R., S. Giovannardi, F. Binda, E. Bossi, and A. Peres. 2002. The relation between charge movement and transport-associated currents in the rat GABA cotransporter rGAT1. *J. Physiol.* 545:739–750.

18. Forster, I., N. Hernando, J. Biber, and H. Murer. 1998. The voltage dependence of a cloned mammalian renal type II Na+/Pi cotransporter (NaPi-2). *J. Gen. Physiol.* 112:1–18.

19. Hager, K., A. Hazama, H. M. Kwon, D. D. Loo, J. S. Handler, and E. M. Wright. 1995. Kinetics and specificity of the renal Na+/myo-inositol cotransporter expressed in Xenopus oocytes. *J. Membr. Biol.* 143:103–113.

20. Kanai, Y., and M. A. Hediger. 2004. The glutamate/neutral amino acid transporter family SLC1: molecular, physiological and pharmacological aspects. *Pflugers Arch.* 447:469–479.

21. Li, M., R. A. Farley, and H. A. Lester. 2000. An intermediate state of the gamma-aminobutyric acid transporter GAT1 revealed by simultaneous voltage clamp and fluorescence. *J. Gen. Physiol.* 115:491–508.

22. Sacher, A., N. Nelson, J. T. Ogi, E. M. Wright, D. D. Loo, and S. Eskandari. 2002. Presteady-state and steady-state kinetics and turnover rate of the mouse gamma-aminobutyric acid transporter (mGAT3). *J. Membr. Biol.* 190:57–73.

23. Virkki, L. V., I. C. Forster, J. Biber, and H. Murer. 2005. Substrate interactions in the human type IIa sodium-phosphate cotransporter (NaPi-IIa). *Am. J. Physiol. Renal Physiol.* 288:F969–F981.

24. Mackenzie, B., D. D. Loo, M. Panayotova-Heiermann, and E. M. Wright. 1996. Biophysical characteristics of the pig kidney Na+/glucose cotransporter SGLT2 reveal a common mechanism for SGLT1 and SGLT2. *J. Biol. Chem.* 271:32678–32683.

25. Parent, L., S. Supplisson, D. D. Loo, and E. M. Wright. 1992. Electrogenic properties of the cloned Na+/glucose cotransporter: I. Voltage-clamp studies. *J. Membr. Biol.* 125:49–62.

26. Gagnon, D. G., P. Bissonnette, and J. Y. Lapointe. 2006. Identification of a disulfide bridge linking the fourth and the seventh extracellular loops of the Na+/glucose cotransporter. *J. Gen. Physiol.* 127:145–158.

27. Bissonnette, P., J. Noel, M. J. Coady, and J. Y. Lapointe. 1999. Functional expression of tagged human Na+-glucose cotransporter in Xenopus laevis oocytes. *J. Physiol.* 520:359–371.

28. Eskandari, S., E. M. Wright, and D. D. Loo. 2005. Kinetics of the reverse mode of the Na+/glucose cotransporter. *J. Membr. Biol.* 204:23–32.

29. Sauer, G. A., G. Nagel, H. Koepsell, E. Bamberg, and K. Hartung. 2000. Voltage and substrate dependence of the inverse transport mode of the rabbit Na(+)/glucose cotransporter (SGLT1). *FEBS Lett.* 469:98–100.

30. Charron, F. M., M. G. Blanchard, and J. Y. Lapointe. 2006. Intracellular hypertonicity is responsible for water flux associated with Na+/glucose cotransport. *Biophys. J.* 90:3546–3554.

31. Chen, X. Z., M. J. Coady, F. Jackson, A. Berteloot, and J. Y. Lapointe. 1995. Thermodynamic determination of the Na+: glucose coupling ratio for the human SGLT1 cotransporter. *Biophys. J.* 69:2405–2414.